Available online at www.sciencedirect.com
SCIENCE DIRECT®
Polymer 44 (2003) 6077–6087
polymer
www.elsevier.com/locate/polymer

Molecular modelling of the elastic behaviour of poly(ethylene terephthalate) network chains

J.I. Cail, R.F.T. Stepto*

Polymer Science and Technology Group, Manchester Materials Science Centre, UMIST and University of Manchester, Grosvenor Street, Manchester M1 7HS, UK

Received 10 February 2003; received in revised form 14 May 2003; accepted 14 May 2003

Dedicated to Professor Ian M. Ward on the occasion of his 75th birthday.

Abstract

The Monte-Carlo (MC) method developed to model the elastomeric stress–strain behaviour of polyethylene (PE) and poly(dimethyl siloxane) (PDMS) networks and the stress–optical behaviour of PE networks is now applied to the stress–strain behaviour of poly(ethylene terephthalate) (PET) networks. In keeping with the previous results for PE and PDMS networks, increases in the proportions of fully extended chains with macroscopic deformation are found to give rise to steady decreases in the rates of Helmholtz energy changes, causing reductions in moduli at moderate macroscopic deformations. There is no need to invoke a transition from affine to phantom chain behaviour as deformation increases.

By using rotational-isomeric-state (RIS) models of the network chains and the MC method, stress–strain behaviour can be related to chemical structure. In this respect, the greater conformational flexibility of the PET chain leads to lower network moduli and smaller deviations from Gaussian network behaviour than for PE networks. In addition, the stiff, aromatic section of the PET repeat unit structure is seen to endow particular characteristics on the end-to-end distribution functions of PET chains. These characteristics are taken fully into account in evaluating the elastomeric properties of the PET networks. Subsequent publications will apply the present results to interpreting the measured stress–strain and the stress–optical properties of entangled PET melts.

Keywords: Elastic behaviour; Polyethylene; Poly(dimethyl siloxane)

1. Introduction

Calculations of elastomeric properties of polymer networks have conventionally used theories and models based on the behaviour of a collection of 'average' chains, with all the chains responding identically to external forces [1–4]. To explain experimental behaviour, such approaches require the unrealistic postulate of a transition from affine to phantom chain behaviour as deformation increases [2–4]. However, a Monte-Carlo (MC) approach, proposed by the present authors and collaborators [5–8], to simulating the stress–strain and stress–optical properties of polymer networks has shown unequivocally that the responses of individual chains have to be accounted for in defining network behaviour and properties. The initial network-chain deformation accompanying sample deformation is affine in the macroscopic strain, giving rise to the experimentally observed initial network modulus, and, as more and more chains reach conformational full extension, the modulus decreases. The postulate of a transition from affine to phantom chain behaviour is not required. Of course, the rapid increase in network modulus at high extensions (before sample rupture), due to the onset of stress-induced crystallisation, or as a result of energy changes associated with valence angle deformation and bond stretching is not treated by the MC approach, nor by an affine to phantom transition.

To date, the MC approach has been applied to poly(dimethyl siloxane) (PDMS) and polyethylene (PE) networks [5–8]. Stress–strain data of Erman and Flory [3] on swollen PDMS networks have been interpreted successfully [5] and, in collaboration with Professor Ward and his colleagues, the classical stress–optical results of Saunders [9] on PE networks have been interpreted quantitatively [7,

* Corresponding author.

0032-3861/03/$ - see front matter © 2003 Published by Elsevier Ltd.
doi:10.1016/S0032-3861(03)00553-6

8]. The present paper applies the MC method to the stress–strain behaviour of poly(ethylene terephthalate) (PET) networks. Subsequent papers will deal with conformational changes on deformation, with stress–optical properties and with modelling the properties of entangled PET melts.

It has been shown previously [10,11] that the conformational behaviour of PET chains in melts does not follow the Williams–Flory (W–F) rotational-isometric-state (RIS) model [12]. That model was derived to describe the conformational behaviour in mixed phenol solvents. For melts, an RIS model with a much lower energy for the gauche conformation about the C–C bond of the glycol segment is needed [10,11]. This model gives agreement with results from new infra-red (IR) spectrometry measurements of conformer populations [13].

2. Geometry of the PET chain and RIS model of PET chains in melts

The *trans*-terephthaloyl and *cis*-terephthaloyl isomers of the six-bond repeat-unit structure used are shown in Fig. 1. The geometrical parameters (bond lengths, l_i, and valence angle supplements, θ_i) taken from Williams and Flory [12], are as follows: $l_1 = l_3 = l_{O-C'} = 0.134$ nm (C′ denotes the carbonyl carbon atom), $l_4 = l_6 = l_{O-C} = 0.144$ nm, $l_5 = l_{C-C} = 0.153$ nm, $l_2 = 0.574$ nm (virtual bond), $\theta_1 = \theta_2 = 66°$, $\theta_3 = \theta_6 = 67°$, and $\theta_4 = \theta_5 = 70°$.

The RIS treatment considers probabilities associated

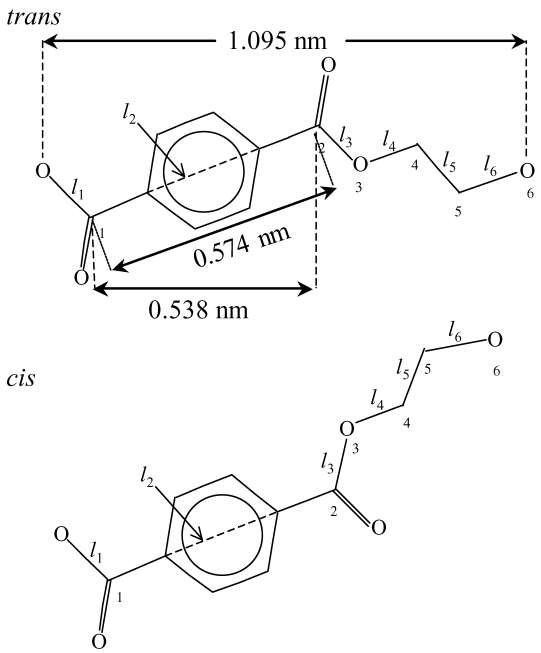

Fig. 1. *Trans* and *cis* PET repeat-unit structures, after Williams and Flory [12]; skeletal atoms are labelled 1–6, and the i th bond connects pairs of atoms with indices i and $i-1$; bond lengths are denoted l_i. The fully extended length of the *trans* repeat unit is 1.095 nm. The length of the virtual bond spanning the aromatic ring is 0.574 nm and its length resolved along the direction of the fully extended *trans* repeat unit is 0.538 nm.

with the rotational states of consecutive pairs of skeletal bonds. The statistical weight, $u_{\eta\zeta;i}$ associated with a rotational state η of skeletal bond i is also dependent upon the state ζ at bond $i-1$. The value of $u_{\eta\zeta;i}$ is related to the corresponding rotational energy, $E_{\eta\zeta;i}$, by

$$u_{\eta\zeta;i} = \exp\left(\frac{-E_{\eta\zeta;i}}{RT}\right). \tag{1}$$

The set of interdependent statistical weights pertaining to all rotational states for a given bond pair can be expressed in the form of a statistical weights matrix $U_i = [u_{\eta\zeta;i}]$, with states ζ for bond $i-1$ indexing the rows and states η for bond i indexing the columns. The statistical weights matrices for the six skeletal bonds of the PET repeat unit (Fig. 1) are listed in the following equations [10].

$$i \neq 2,3; \qquad U_i = \begin{bmatrix} & g_- & t & g_+ \\ g_- & & & \\ t & & & \\ g_+ & & & \end{bmatrix};$$

$$U_2 = \begin{bmatrix} & cis & trans \\ g_- & & \\ t & & \\ g_+ & & \end{bmatrix}; \qquad U_3 = \begin{bmatrix} & g_- & t & g_+ \\ cis & & & \\ trans & & & \end{bmatrix}$$

$$U_1 = \begin{bmatrix} 0 & 1 & 0 \\ 0 & 1 & 0 \\ 0 & 1 & 0 \end{bmatrix} \tag{2}$$

$$U_2 = \begin{bmatrix} 0 & 0 \\ 1 & 1 \\ 0 & 0 \end{bmatrix} \tag{3}$$

$$U_3 = \begin{bmatrix} 0 & 1 & 0 \\ 0 & 1 & 0 \end{bmatrix} \tag{4}$$

$$U_4 = \begin{bmatrix} 0 & 0 & 0 \\ \sigma_4 & 1 & \sigma_4 \\ 0 & 0 & 0 \end{bmatrix} \tag{5}$$

$$U_5 = \begin{bmatrix} \sigma_5 & 1 & \sigma_5\omega \\ \sigma_5 & 1 & \sigma_5 \\ \sigma_5\omega & 1 & \sigma_5 \end{bmatrix} \tag{6}$$

$$U_6 = \begin{bmatrix} \sigma_6 & 1 & \sigma_6\omega \\ \sigma_6 & 1 & \sigma_6 \\ \sigma_6\omega & 1 & \sigma_6 \end{bmatrix} \tag{7}$$

The model has *gauche* conformational states of bonds 4–6 at $\phi_{g\pm} = \pm 120°$.

The energies [11] associated with the statistical weights

$\sigma_4 = \sigma_6$, σ_5 and ω are $E_{\sigma 4} = E_{\sigma 6} = 1.75\ \text{kJ mol}^{-1}$, $E_{\sigma 5} = -4.16\ \text{kJ mol}^{-1}$ and $E_\omega = 5.80\ \text{kJ mol}^{-1}$. The value of $E_{\sigma 5} = -4.16\ \text{kJ mol}^{-1}$ gives, at 523 K, the characteristic ratio $(\langle r^2\rangle/M)_\infty = 6.94 \times 10^{-3}\ \text{nm}^2$ and 76.4% gauche conformers about bond 5. This value of $(\langle r^2\rangle/M)_\infty$ is consistent with experimental values for PET melts at 523 K [14] of $6.14–6.94 \times 10^{-3}\ \text{nm}^2$. The value of $E_{\sigma 5} = -4.16\ \text{kJ mol}^{-1}$ also gives 76% gauche conformers at 541 K, consistent with measured values [13]. On the other hand, a value of $E_{\sigma 5} = -5.84\ \text{kJ mol}^{-1}$ is needed to give $(\langle r^2\rangle/M)_\infty = 6.14 \times 10^{-3}\ \text{nm}^2$. This energy value is too low as it also predicts about 81% gauche conformers at 541 K. The value of $E_{\sigma 5} = -1.02\ \text{kJ mol}^{-1}$ used by Williams and Flory, for PET in mixed phenol solvents, gives $9.60 \times 10^{-3}\ \text{nm}^2$ and about 61% gauche conformers at 523 K.

3. Modelling chain conformational behaviour and elastic free-energy [5,6]

In the first stage of the MC calculations, the RIS PET chain model is used to generate radial end-to-end distance distributions, $W(r)$, for unperturbed chains of various numbers of skeletal bonds (n) at a given temperature. The populations of conformations are generated using conditional probabilities to grow chains bond-by-bond linked with Metropolis acceptance criteria for efficient sampling [5,6]. The radial end-to-end distributions are constructed as histograms for the MC samples generated. The corresponding values of probability density, $P(\boldsymbol{r})$, are evaluated as $W(r)/4\pi r^2$, assuming the random orientation of chains in three dimensions.

The second stage of the simulations concerns the elastic behaviour of networks. A network is represented by a sample of independent, spherically symmetrical individual chains in a Cartesian laboratory-reference frame; one end of each chain is fixed at the origin. The chains are deformed uniaxially by a deformation ratio, $\boldsymbol{\lambda}$, with $\lambda_x\lambda_y\lambda_z = 1$ (i.e. constancy of volume). The end-to-end distances are allowed to increase only up to their effective, conformational maximum, $r^*_{\max}$, above which $W(r) = 0$ according to the sampled $W(r)$. For an individual polymer chain in a network, the Helmholtz energy change upon deformation at an absolute temperature, T, is assumed to arise solely from the corresponding entropic change. Hence,

$$\Delta A_{\text{chain}}/kT = \ln\{P(r_o)/P(r_{\text{def}})\}, \tag{8}$$

where the subscripts 'o' and 'def' denote the relaxed and deformed end-to-end vectors, respectively.

In the deformation scheme, a chain with end-to-end distance r_o is first chosen in proportion to $W(r_o)$. The X- and Y- co-ordinates of its 'free' chain end are chosen randomly, and the Z-component defined consistent with $\boldsymbol{r}_o$. Uniaxial deformations, using a series of values of λ are applied in the Z-direction (i.e. $\lambda = \lambda_z$) and the deformed end-to-end distances calculated by simple geometry, with $\lambda_x = \lambda_y = 1/\sqrt{\lambda}$. Any values of r_{def} in excess of $r^*_{\max}$ are put equal to $r^*_{\max}$, thus limiting r to the range of values determined by the bond-conformational energies and consistent with $W(r)$. The associated value of $W(r_{\text{def}})$ is ascertained from $W(r)$, and $\ln P(\boldsymbol{r}_{\text{def}})$ evaluated. The Helmholtz energy change is evaluated via Eq. (8), and the average change per chain at each λ calculated as

$$\Delta A/NkT = \frac{1}{N}\sum_{i=1}^{N} \ln\{P(\boldsymbol{r}_o)/P(\boldsymbol{r}_{\text{def}})\}, \tag{9}$$

where N is the number of chains in the MC sample (i.e. network). Typically, $N = 3$ to 5×10^6. In addition,

$$\langle r^2_{\text{def}}\rangle = \frac{1}{N}\sum_{i=1}^{N} r^2_{o,i} \tag{10}$$

is calculated and the proportion of chains reaching conformational full extension ($r = r^*_{\max}$) recorded.

4. Results

4.1. Individual chain behaviour

4.1.1. Evaluation of equivalent freely jointed chains

In order that simulated end-to-end distributions and elastic behaviour can be compared with Gaussian-based models [1], the parameters of the equivalent freely jointed chains for the RIS PET chains being studied need to be defined. It also helps the interpretation of elastic behaviour to see how the chemical structure of PET is reflected in the parameters of these equivalent freely jointed chains, and how the parameters compare with those of PE and PDMS.

The conventional Kuhn treatment [1], where the equivalent freely jointed chain (m links of length l') is forced to adopt the same mean-square and maximum end-to-end distance, $\langle r^2\rangle$ and $r_{\max}$ as those of the real chain (of n skeletal bonds),

$$\langle r^2\rangle = ml'^2 \tag{11}$$

$$r_{\max} = ml' \tag{12}$$

is used to compare the PE and PET chains. Eqs. (11) and (12) allow m and l' to be evaluated from

$$m = \frac{r^2_{\max}}{\langle r^2\rangle} \tag{13}$$

$$l' = \frac{\langle r^2\rangle}{r_{\max}} \tag{14}$$

Eq. (13) also enables the useful characteristic ratio, the number of actual skeletal bonds per freely jointed link, to be evaluated with

$$\frac{n}{m} = n\frac{\langle r^2\rangle}{r^2_{\max}} \tag{15}$$

Further, $\langle r^2 \rangle$ may be expressed by the equation,

$$\langle r^2 \rangle = nb^2 \tag{16}$$

where b is the (root-mean-square) effective bond length.

For a particular chain, $\langle r^2 \rangle$ is found from the RIS model, using Flory's matrix algebraic methods of calculation [15] or the MC simulations of $W(r)$, with $\langle r^2 \rangle = \sum_{i=1}^{N} r^2 W(r)$. The MC samples were in fact chosen so that they gave $\langle r^2 \rangle$ to within 0.1% of the exact values calculated via matrix algebra. For PE, the RIS model of Abe, Jernigan and Flory [15] was used [6] to calculate $\langle r^2 \rangle$ and $r_{max} = nl\cos(\theta/2)$, where $l = 0.153$ nm is the C–C bond length and $\theta = 68°$ the supplement of the ∠CCC valence angle. For PET, the RIS model used to calculate $\langle r^2 \rangle$ was as defined in Section 2 and Fig. 1 shows that

$$r_{max}/\text{nm} = \frac{n}{6}1.095. \tag{17}$$

For PDMS, r_{max} is not uniquely defined, owing to the occurrence of alternating unequal O and Si valence angles. Hence, a moment-ratio method has to be used to define average values of m and l' for the PDMS chain. The method is discussed in detail elsewhere [6] and will not be considered further here. However, Eq. (16) is valid for PDMS chains and will be used in the present comparisons of chain structure and conformational behaviour.

Fig. 2(a) shows n/m for PE chains at 298 K and PET chains at 298 and 523 K. As discussed previously, the latter temperature is the temperature at which $(\langle r^2 \rangle/M)_\infty$ of PET melts was measured [14] and is used in the present paper for the calculations of elastic behaviour. For PET, the change in n/m with temperature is small and positive (equivalent to $\mathrm{d}\ln\langle r^2 \rangle/\mathrm{d}T \approx 0.7 \times 10^{-3}\ \mathrm{K}^{-1}$) due to the flexible, long virtual bond (Fig. 1), of length l_2, bridging the benzene ring, together with the predicted [15] small increase with temperature of the dimensions of the ethylene oxide units in the chain. The flexibility of the virtual bond is evident from the statistical-weights matrix U_2 (Eq. (3)), according to which the *trans* and *cis* isomers occur with equal weight. Further, Fig. 2(a) shows that PET is, conformationally, a much more flexible chain than PE, with only about seven real bonds required to span the freely jointed link, whose average orientation is unrelated to those of its predecessors and successors along the chain. The larger conformational flexibility (small value of n/m) of PET is further reflected in the smaller values of l'^2 shown in Fig. 2(b). The percentage change in l'^2 for 298–523 K is about twice that in n/m as the former quantity is proportional to $\langle r^2 \rangle^2$ and the latter quantity proportional to $\langle r^2 \rangle$.

Fig. 2(c) gives values of b^2 for PET, PE and PDMS chains. b^2 is basically a measure of molecular size per skeletal bond. The plots show that PET is the largest chain of the three, and PDMS is the smallest. Also, the values of b^2 for PET and PDMS are relatively insensitive to n as both are conformationally more flexible than PE. PDMS is smaller than PE because the effects of this

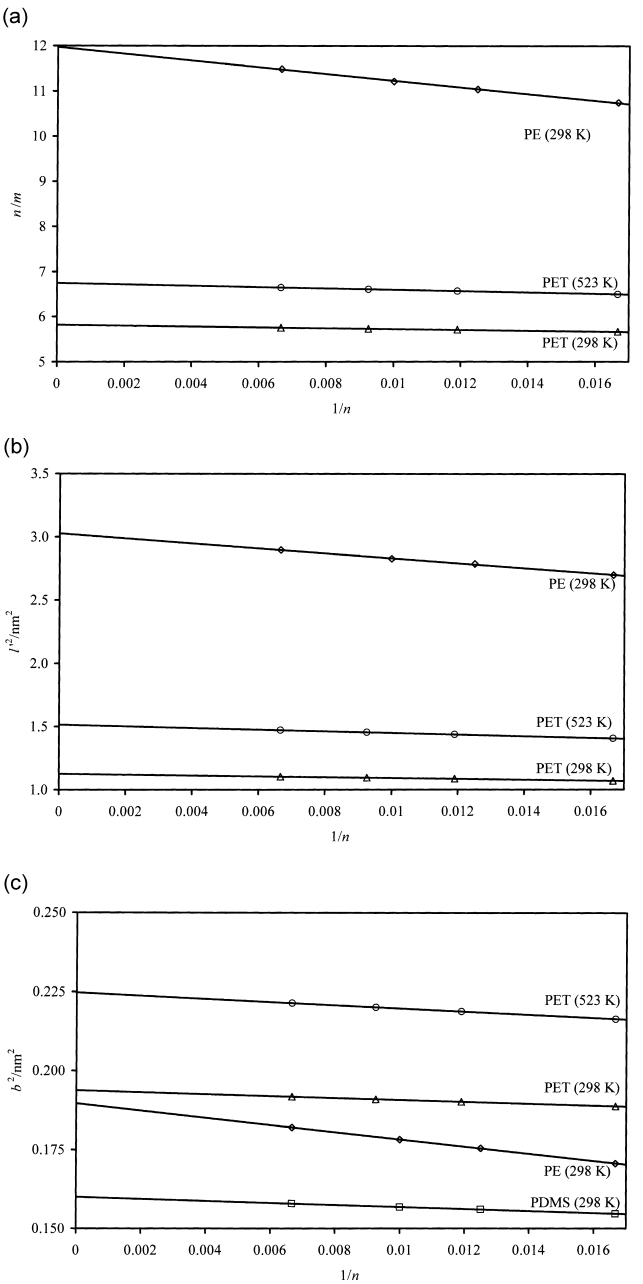

Fig. 2. Parameters of equivalent freely jointed chains as functions of reciprocal number of real skeletal bonds, $1/n$; (a) number of skeletal bonds, n, per equivalent freely jointed link, m, for PE chains at 298 K and PET chains at 298 and 523 K; (b) square of the equivalent freely jointed link length, l'^2, for PE chains at 298 K and PET chains at 298 K and 523 K; (c) mean-square end-to-end distance per skeletal bond, b^2, for PE and PDMS chains at 298 K and PET chains at 298 and 523 K.

flexibility outweigh its longer skeletal bond length (Si–O cf. C–C) and wider O–Si–O valence angle (cf. CCC valence angle). With PET, the effects of the extremely long virtual bond dominate. Fig. 1 shows that its resolved length (0.538 nm) is about one half the fully extended length of the PET repeat unit (1.095 nm).

The overall picture that emerges from this comparison of

equivalent-chain behaviour is that PET has a relatively long and conformationally flexible chain structure.

4.1.2. Radial distribution functions

Fig. 3 shows $W(r/r_{max}) = W(r) \times r_{max}$ plotted as a function of r/r_{max} for PET chains of 84- and 150-bonds and a PE chain of 150-bonds. The distribution for PE was generated [6] using histograms divided into 20 intervals between $r = 0$ and $r = r_{max}$. For chains of 150 bonds, it can be seen that the distribution for PET ($m = 22.6$) is much narrower than that for PE ($m = 13.3$), as a consequence the distribution curve for PET rises and falls much more rapidly with r/r_{max}. Hence, for the PET calculations it was necessary to increase the number of histogram intervals to 200 between $r = 0$ and $r = r_{max}$ to account accurately for the initial and final curvatures in the distribution functions. When the 150-bond PE chain is compared with a PET chain of 84-bonds ($m = 12.8$) the distributions are much closer together, as would be expected from their similar values of m. However, there are differences between the two distributions. The PET distribution peaks at a higher value of r/r_{max} as $r \to 0$ and as $r \to 0$ the values of $W(r)$ are smaller for the PET distribution. The smaller population of conformations as $r \to 0$ is probably due to the long virtual bond (of length l_2) excluding conformations at small values of r.

4.1.3. Probability density distribution functions ($P(r)$)

Fig. 4 shows $\ln P(\boldsymbol{r})$ versus $(r/r_{max})^2$ for the same chains as in Fig. 3, with $P(\boldsymbol{r})$ evaluated from

$$P(\boldsymbol{r}) = \frac{W(r)}{4\pi r^2}. \tag{18}$$

Considering first the behaviour as $\boldsymbol{r} \to \boldsymbol{0}$, the distributions give the values of $\ln(P(\boldsymbol{r}))$ at $\boldsymbol{r} = \boldsymbol{0}$ expected from the

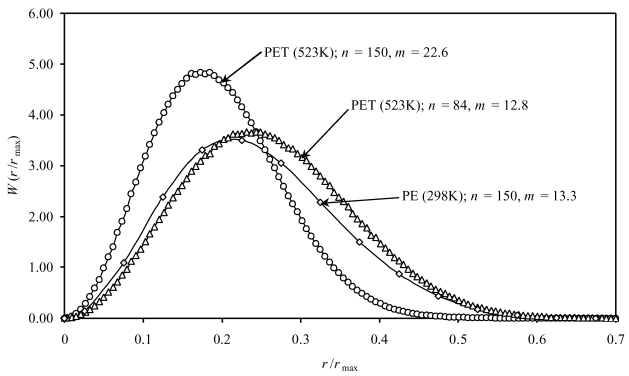

Fig. 3. Radial distribution function, $W(r/r_{max}) = W(r) \times r_{max}$, versus r/r_{max} for PET chains of 84 and 150 bonds at 523 K and a PE chain of 150 bonds at 298 K. The areas under the curves shown are normalised to unity. For PET $n = 84$, $r_{max} = 15.3$ nm, for PET $n = 150$, $r_{max} = 27.4$ nm and for PE, $n = 150$, $r_{max} = 19.0$ nm.

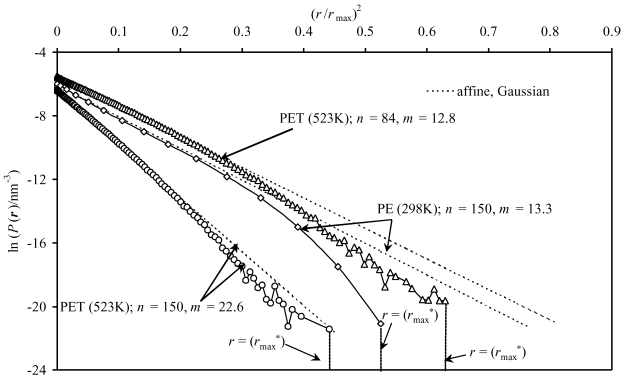

Fig. 4. $\ln P(\boldsymbol{r})$ versus $(r/r_{max})^2$ for PET chains of 84 and 150 bonds at 523 K and PE chains of 150 bonds at 298 K.

equivalent Gaussian distributions, namely,

$$(P(\boldsymbol{r}))_{Gaussian} = \left(\frac{3}{2\pi\langle r^2\rangle}\right)^{3/2} \exp\left(\frac{-3r^2}{2\langle r^2\rangle}\right) \tag{19}$$

with $\ln P(\boldsymbol{0}) = \ln(3/2\pi\langle r^2\rangle)^{3/2}$.

As r increases towards r^*_{max}, the PET distributions show some undulations. Again, this behaviour may be attributed to the effects of the large flexible virtual bond in the PET structural unit giving relatively higher and lower probabilities of particular values of r. The PE distribution ($n = 150$, $m = 13.3$) drops more steeply and finishes at a lower value of r/r_{max} than that for the PET distribution for $n = 84$ ($m = 12.8$). It should be recalled that the distributions finish when $r = r^*_{max}$, with r^*_{max} the largest simulated value of r for which $W(r) > 0$.

The steeper slope in Fig. 4 from the PE distribution means that, compared with PET, at a similar value of m, there will be a larger drop in entropy and a larger increase in free energy (cf. Eqs. (8) and (9)) as a chain is extended between two given values of $(r/r_{max})^2$. The effects of these differences will be apparent in the following sections when changes in Helmholtz energy resulting from network deformation are considered.

4.2. Elastic behaviour of networks of PET chains

4.2.1. Analysis of $\langle r^2_{def}\rangle$

For the macroscopic, uniaxial, affine deformation of an assembly of chains, with no limit on maximum chain extension and with no volume change [1]

$$\langle r^2_{def}\rangle = \frac{\langle r^2_o\rangle}{3}(\lambda^2 + 2/\lambda). \tag{20}$$

Eq. (20) refers to uniaxial extension or compression. However, assuming that λ in the equation refers to uniaxial extension, the conjugate uniaxial compression ratio, λ^* (<1), that produces the same value of $\langle r^2_{def}\rangle$ as λ (>1), is related to λ by the expression [5,6]

$$\lambda^* = \frac{\lambda}{2}[(1 + 8/\lambda^3)^{1/2} - 1]. \tag{21}$$

Accordingly, the maximum extension ratio considered here, $\lambda \approx 2.5$, corresponds to $\lambda^* = 0.29$ in uniaxial compression.

$\langle r^2_{def}\rangle/\langle r^2_o\rangle$ for networks of 60-bond to 150-bond PET chains and a for a network of 150-bond PE chains, determined using Eq. (10), are plotted versus $\lambda^2 + 2/\lambda - 3$ in Fig. 5(a) and (b) for extension and in Fig. 6(a) and (b) for compression. Two scales in $\lambda^2 + 2/\lambda - 3$ are shown in each case; a value of $\lambda = 2.5$ corresponds to $\lambda^2 + 2/\lambda - 3 = 4.05$ and $\lambda = 1.46$ corresponds to $\lambda^2 + 2/\lambda - 3 = 0.50$. The affine, Gaussian behaviour of Eq. (20) results in the dashed lines shown of slope = 1/3. It can be seen that generally the $\langle r^2_{def}\rangle$ begins to depart noticeably from affine behaviour at $\lambda^2 + 2/\lambda - 3 \approx 0.04$, corresponding to $\lambda \approx 1.12$ in extension and $\lambda^* \approx 0.89$ in compression. The non-affine behaviour at larger deformations is due to the finite extensibility of individual network chains, with the PE network showing larger deviations and the PET networks showing increasing deviations as chain length decreases. The PE network chains show initial deformations that are very slightly larger than affine, which may be due to numerical uncertainties. As expected, and as found previously for PE and PDMS network chains [5,6], there are larger deviations in uniaxial extension than in uniaxial compression. (Uniaxial compression by λ is equivalent to an equi-biaxial extension by $\lambda^{-1/2}$.)

Fig. 7(a) and (b) shows the fractions of chains reaching conformational full extension ($r_{def} = r^*_{max}$). These fractions are responsible for the non-affine behaviour shown in Figs. 5 and 6. The curves for PET $n = 60$ are not shown because of the uncertainties in determining r^*_{max} at short chain lengths. (Even larger fluctuations in $\ln(P(\boldsymbol{r}))$ versus $(r/r_{max})^2$ occurred for this chain length than those shown for $n = 84$ in Fig. 4). It

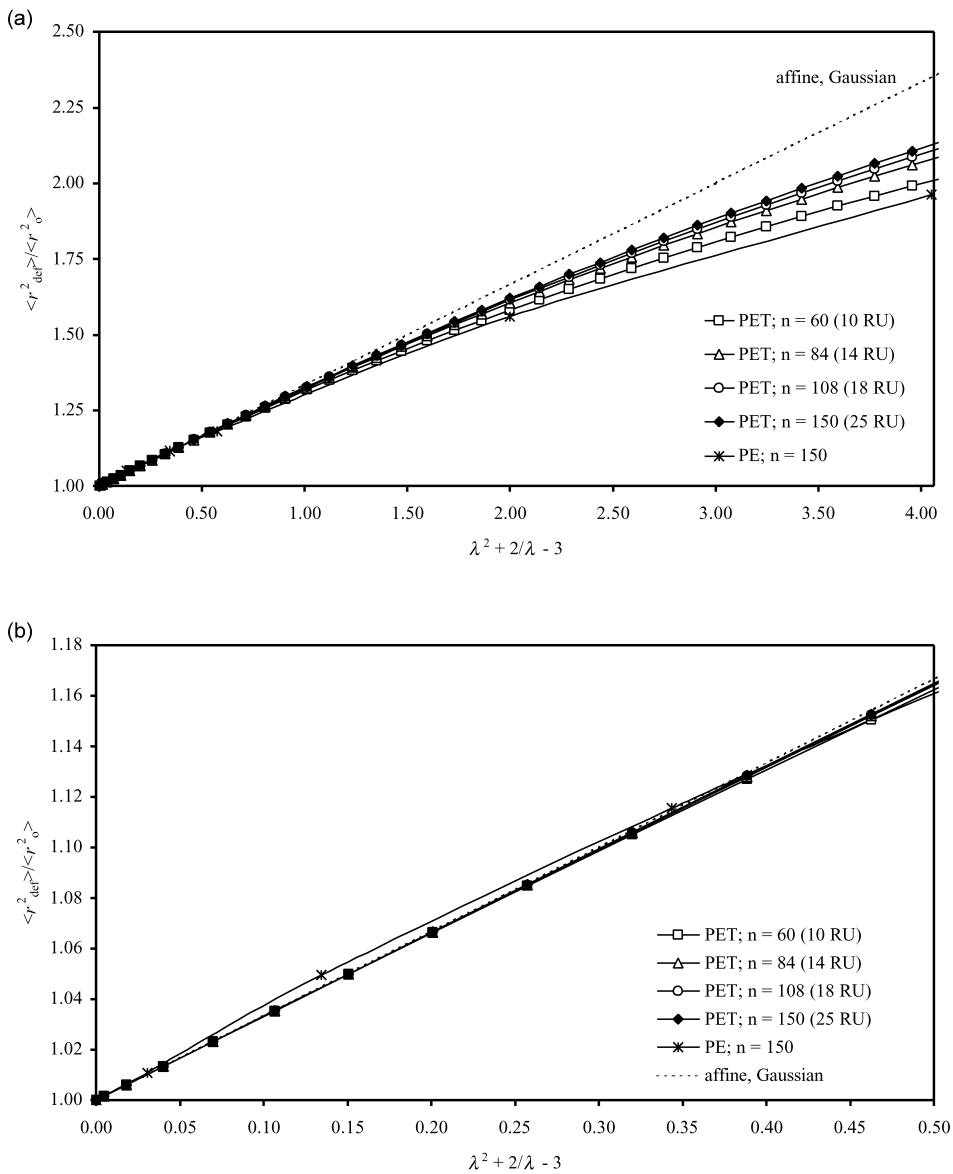

Fig. 5. $\langle r^2_{def}\rangle/\langle r^2_o\rangle$ versus $\lambda^2 + 2/\lambda - 3$ for networks of PET chains of 60, 84, 108 and 150 skeletal bonds at 523 K and for a network of PE chains of 150 skeletal bonds at 298 K under uniaxial extension, (a) $\lambda^2 + 2/\lambda - 3$ from 0.0 to 4.0 and (b) $\lambda^2 + 2/\lambda - 3$ from 0.0 to 0.5. (RU = repeat unit.).

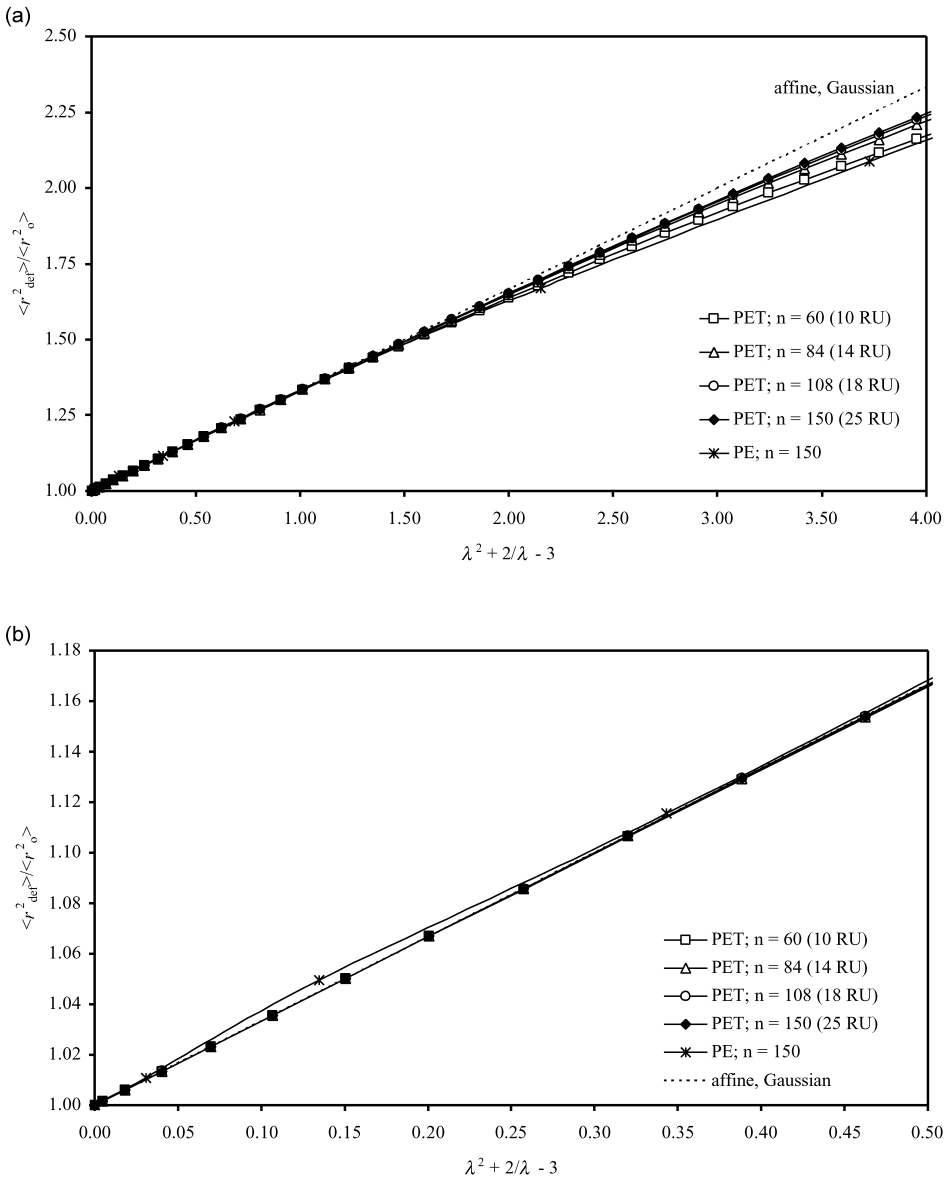

Fig. 6. $\langle r^2_{def}\rangle/\langle r^2_o\rangle$ versus $\lambda^2 + 2/\lambda - 3$ for networks of PET chains of 60, 84, 108 and 150 skeletal bonds at 523 K and for a network of PE chains of 150 skeletal bonds at 298 K under uniaxial compression, (a) $\lambda^2 + 2/\lambda - 3$ from 0.0 to 4.0 and (b) $\lambda^2 + 2/\lambda - 3$ from 0.0 to 0.5.

can be seen that relatively small percentages of fully extended chains are responsible for significant departures from affine behaviour and, consistent with the larger deviations from affine behaviour for PE shown in Figs. 5 and 6, larger proportions of the PE network chains are conformationally fully extended. As expected, for the PET network chains, the percentage of conformationally fully extended chains decreases as chain length increases. Also, uniaxial compression results in fewer fully extended chains than does uniaxial extension.

4.2.2. Helmholtz energy change

The network Helmholtz energy change accompanying a macroscopic uniaxial deformation of λ, with no volume change, can be expressed as [5,6]

$$\Delta A/NkT = s(\lambda^2 + 2/\lambda - 3). \quad (22)$$

For Gaussian (affine) networks [1], $s = 1/2$, and a plot of $\Delta A/NkT$ versus $\lambda^2 + 2/\lambda - 3$ for uniaxial extension and compression is linear with a slope of 1/2.

As far as the changes in Helmholtz energy are concerned, the non-affine network chain behaviour described in Section 4.2.1 can be viewed as a kind of orientation effect. Chains in the relaxed network, whose end-to-end vectors lie close to the extension axis become conformationally fully extended at low macroscopic strains, and hence contribute nothing more to the Helmholtz energy change of the network as deformation increases further; more of the strain is effectively 'taken-up' by network chains whose end-to-end vectors lie at ever-increasing angles from the extension

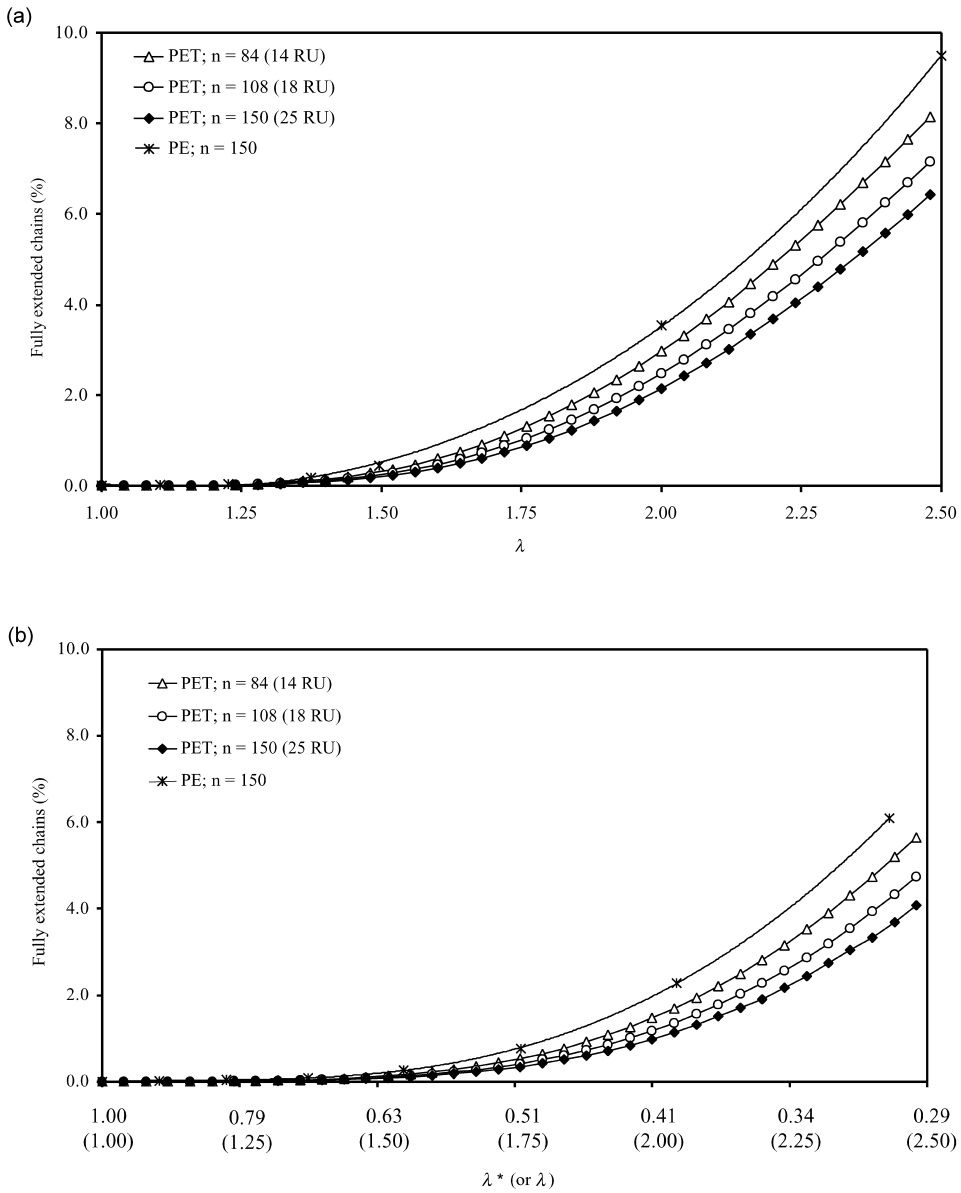

Fig. 7. Percentage of conformationally fully extended chains as a function of macroscopic uniaxial deformation, λ, for networks of PET chains of 84, 108 and 150 skeletal bonds at 523 K and for a network of PE chains of 150 skeletal bonds at 298 K, under (a) uniaxial extension and (b) uniaxial compression.

axis. The phenomenon manifests itself as a reduction in the rate of Helmholtz energy change per chain with increasing macroscopic deformation.

The energy changes on deformation to given values of λ were evaluated using Eq. (9). The results in extension are shown versus $\lambda^2 + 2/\lambda - 3$ in Fig. 8(a) and (b) and those in compression in Fig. 9(a) and (b). Again, two scales in $\lambda^2 + 2/\lambda - 3$ are shown in each case. The smaller scale, up to $\lambda^2 + 2/\lambda - 3 = 4.00$ is the same as that used in Figs. 5(a) and 6(a). $\lambda = 1.28$ corresponds to $\lambda^2 + 2/\lambda - 3 = 0.20$ (Fig. 8(b)) and $\lambda = 1.41$ corresponds to $\lambda^2 + 2/\lambda - 3 = 0.40$ (Fig. 9(b)). Results for PET networks of 60-, 84-, 108- and 150-bond chains and for PE networks of 60- and 150-bond chains are shown. Overall, there are smaller deviations from Gaussian behaviour in compression than in extension. Also, the PET networks show smaller deviations than the PE networks and ΔA is less sensitive to chain length. Such comparative behaviour is consistent with the distributions of Fig. 4, in that the slopes of the PET curves are nearer to the Gaussian slopes than is the slope of the PE curve. The contributions from individual chain deformations that are summed to give ΔA (Eq. (9)) are equal to *differences* in ordinates between pairs of points on the curves shown in Fig. 4. Hence, deviations from Gaussian behaviour in ΔA relate to the differences between the *slopes* of the curves in Fig. 4 and the slopes of the Gaussian lines. However, it should be remembered that there is not a unique relationship between the slope and ΔA because r for an individual chain and λ can subtend any angle to each

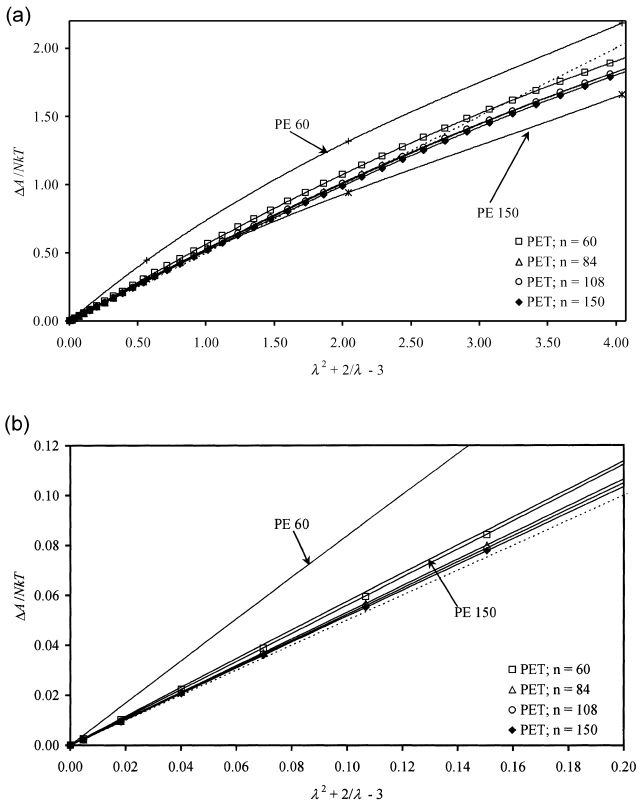

Fig. 8. Helmholtz energy change per chain ($\Delta A/NkT$) as a function of $\lambda^2 + 2/\lambda - 3$ for networks of PET chains of 60, 84, 108 and 150 skeletal bonds at 523 K and for a network of PE chains of 150 skeletal bonds at 298 K under uniaxial extension; (a) $\lambda^2 + 2/\lambda - 3$ from 0.0 to 4.0 and (b) $\lambda^2 + 2/\lambda - 3$ from 0.0 to 0.2. --- affine, Gaussian behaviour.

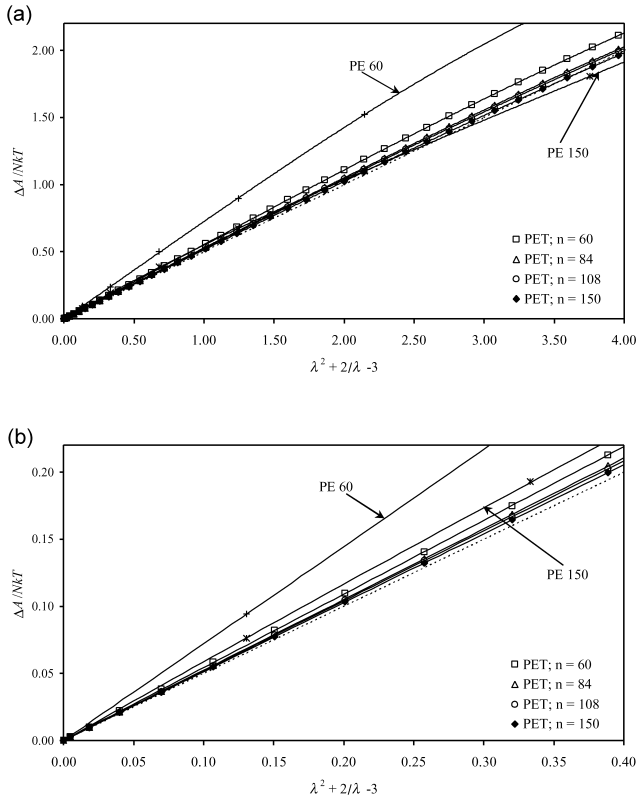

Fig. 9. Helmholtz energy change as a function of $\lambda^2 + 2/\lambda - 3$ for networks of PET chains of 60, 84, 108 and 150 skeletal bonds at 523 K and for a network of PE chains of 150 skeletal bonds at 298 K under uniaxial compression; (a) $\lambda^2 + 2/\lambda - 3$ from 0.0 to 4.0 and (b) $\lambda^2 + 2/\lambda - 3$ from 0.0 to 0.4. --- affine, Gaussian behaviour.

other and, in addition, extension of an individual chain beyond $r = r^*_{max}$ cannot occur.

Generally, at small deformations, the chains show larger Helmholtz energy changes than expected for freely jointed Gaussian chains. As deformation increases and some chains reach conformational full extension, the rate of change of Helmholtz energy decreases and eventually, in all cases, ΔA will fall below the Gaussian values. Inspection of the results in Figs. 8 and 9 show that shorter PET chains start with higher values of ΔA. If the abscissae were extended, the values of ΔA would eventually, in all cases, lie below the Gaussian line and in fact be smaller for shorter chain lengths as more chains become fully extended. The curves plotted for the stiffer PE chains lie above those for the PET chains at smaller deformations but show larger decreases in their rates of change of ΔA with deformation, so that at larger deformations the curves for PE, $n = 150$, fall below those for PET.

4.2.3. Stress–strain behaviour

The normalised Helmholtz energy change in Eq. (22) can be expressed in terms of the density, ρ, and volume, V, of the unswollen network:

$$\frac{\Delta A}{RT\rho}\frac{1}{V} = \frac{s}{M_c}(\lambda^2 + 2/\lambda - 3) \tag{23}$$

where R is the universal gas constant and M_c is the network-chain molar mass. In general, s is a function of λ. Differentiation of Eq. (23) with respect to sample length, l, yields the normalised retractive force, $f/RT\rho$:

$$\frac{f}{RT\rho}\frac{1}{V} = \frac{1}{l_o M_c}\left[2s(\lambda - 1/\lambda^2) + (\lambda^2 + 2/\lambda - 3)\frac{ds}{d\lambda}\right] \tag{24}$$

where l_o is the initial sample length. The normalised, nominal stress, $\sigma/RT\rho$, can then be found by using the relationship $a_o l_o = V$, where a_o is the initial sample cross-sectional area. Thus,

$$\frac{\sigma}{RT\rho} = \frac{f}{RT\rho a_o} = \frac{1}{M_c}\left[2s(\lambda - 1/\lambda^2) + (\lambda^2 + 2/\lambda - 3)\frac{ds}{d\lambda}\right] \tag{25}$$

$\sigma/RT\rho$ is plotted versus λ in Fig. 10 for PET networks of chain lengths 60 and 150 bonds and for PE networks of chain length 150 bonds. The Gaussian curves are also shown. They were calculated via Eq. (25) with $s = 1/2$ and

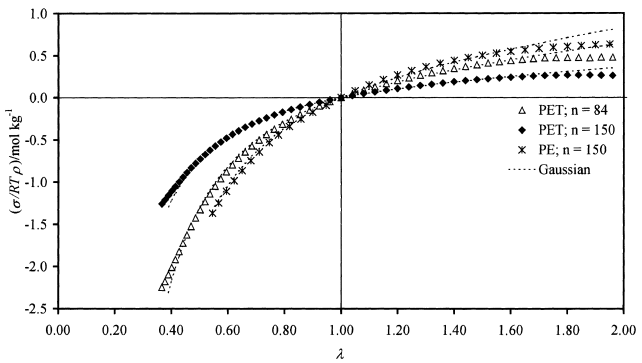

Fig. 10. Normalised nominal stress, $\sigma/RT\rho$, as a function of macroscopic uniaxial deformation, λ, for networks of PET chains of 84 and 150 skeletal bonds at 523 K and for a network of PE chains of 150 skeletal bonds at 298 K. The dashed curves represents affine, Gaussian behaviour. (The curves for PET $n = 60$ and 108 are not shown as they overlap with and partially obscure the curves plotted in the figure.).

$ds/d\lambda = 0$. As expected from the Helmholtz energy plots in Figs. 8 and 9, the deviations are greater in extension than in compression. The 150-bond PE network shows larger deviations from Gaussian behaviour in extension than the 150-bond PET network. However, as can be deduced from the different curvatures of the ΔA plots in Fig. 8, the relative deviations depend on the range of deformations considered.

The values of $\sigma/RT\rho$ can be converted [1,5,6] to reduced normalised stress, $[\sigma^*]/RT\rho$, with

$$\frac{[\sigma^*]}{RT\rho} = \frac{\sigma}{RT\rho(\lambda - 1/\lambda^2)}. \tag{26}$$

Plots of $[\sigma^*]/RT\rho$ versus $1/\lambda$ give Mooney–Rivlin plots. Such plots show more clearly the deviations from Gaussian behaviour. The reduced normalised stress (reduced modulus) for a Gaussian network is equal to $1/M_c$ and is constant at all λ. Fig. 11 shows the Mooney–Rivlin plots for the PET networks and for the 150-bond PE network. In each case, the intercept at $\lambda = 1$ is greater than the Gaussian value. This behaviour follows directly from the initial values of ΔA in Fig. 8 being larger than the Gaussian values. The values for the PET networks are closer to the Gaussian values than that for the PE network. Within the PET networks, curvature decreases as chain length increases. At a given value of $1/\lambda$, the curve for the PET chain with $n = 84$ ($m = 12.8$) shows a smaller decrease in $[\sigma^*]/RT\rho$ than does that for the PE chain ($m = 13.3$), although the reductions below their respective Gaussian values are about the same, consistent with the behaviour shown in Fig. 10.

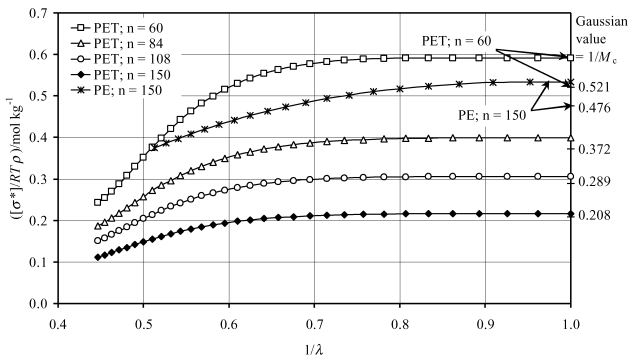

Fig. 11. Mooney–Rivlin plots for networks of PET chains of 60, 84, 108 and 150 skeletal bonds at 523 K and for a network of PE chains of 150 skeletal bonds at 298 K. The values predicted by Gaussian behaviour are indicated.

5. Conclusions and further work

In keeping with the results of previous investigations of the stress–strain behaviour of PE and PDMS networks [5,6], the MC method shows that for PET networks a decrease in the rate of Helmholtz energy change in the deforming network occurs naturally as an increasing proportion of network chains becomes fully extended. The concepts of a phantom network and junction-point fluctuations [2,3] are not required.

By using the MC method and RIS models of network chains, one is able to explain stress–strain behaviour in relation to chemical structure. This paper clearly shows that networks of PET chains have lower moduli and smaller deviations from Gaussian behaviour than those of PE chains of similar numbers of equivalent freely jointed links. The distinction relates directly to the greater conformational flexibility of the PET chain structure, notwithstanding the effects of the long (virtual) bond bridging the benzene ring in PET on $W(r)$ and $P(r)$ at small and large values of r.

Subsequent publications will apply the present results to modelling the measured stress–strain behaviour of PET melts and will further develop the MC method to interpret their stress–optical properties. The conformational properties due specifically to the long virtual bond in the PET chain also need further investigation.

Acknowledgements

The support of the EPSRC is gratefully acknowledged and also access to the Accelrys Polymer software for the background RIS calculations.

References

[1] Treloar LRG. The physics of rubber elasticity, 3rd ed. Oxford: Oxford University Press; 1975.
[2] Flory PJ. Proc R Soc London Ser 1976;A351:351.
[3] Erman B, Flory PJ. Macromolecules 1983;16:1607.
[4] Mark JE, Erman B. In: Stepto RFT, editor. Polymer networks – principles of their formation structure and properties. London: Blackie Academic and Professional; 1998. Chapter 7.
[5] Stepto RFT, Taylor DJR. Macromol Symp 1995;93:261.

[6] Stepto RFT, Taylor DJR. J Chem Soc Faraday Trans 1995;91:2639.
[7] Taylor DJR, Stepto RFT, Jones RA, Ward IM. Macromolecules 1999; 32:1978.
[8] Cail JI, Taylor DJR, Stepto RFT, Brereton MG, Jones RA, Ries ME, Ward IM. Macromolecules 2000;33:4966.
[9] Saunders DW. Trans Faraday Soc 1954;50:881.
[10] Taylor DJR, Stepto RFT, Bleackley M, Ward IM. Phys Chem Chem Phys 1999;1:2065.
[11] Cail JI, Stepto RFT, Taylor DJR, Jones RA, Ward IM. Phys Chem Chem Phys 2000;2:4361.
[12] Williams AD, Flory PJ. J Polym Sci 1967;5(A-2):417.
[13] Saunders LS, Ward IM, Cail JI, Stepto RFT, to be published.
[14] Gilmer JW, Wiswe D, Zachmann H-G, Kugler J, Fischer EW. Polymer 1986;27:1391.
[15] Flory PJ. Statistical mechanics of chain molecules. New York: Wiley Interscience; 1969.